01 Jan 2023

In Situ High-Temperature Raman Spectroscopy Via a Remote Fiber-Optic Raman Probe

Bohong Zhang

Hanok Tekle

Ronald J. O'Malley
Missouri University of Science and Technology, omalleyr@mst.edu

Jeffrey D. Smith
Missouri University of Science and Technology, jsmith@mst.edu

et. al. For a complete list of authors, see https://scholarsmine.mst.edu/matsci_eng_facwork/2925

Recommended Citation

B. Zhang et al., "In Situ High-Temperature Raman Spectroscopy Via a Remote Fiber-Optic Raman Probe," *IEEE Transactions on Instrumentation and Measurement*, vol. 72, article no. 6002008, Institute of Electrical and Electronics Engineers, Jan 2023.
The definitive version is available at https://doi.org/10.1109/TIM.2023.3244238

In Situ High-Temperature Raman Spectroscopy via a Remote Fiber-Optic Raman Probe

Bohong Zhang, Hanok Tekle, Ronald J. O'Malley, Jeffrey D. Smith, Rex E. Gerald II, and Jie Huang, *Senior Member, IEEE*

***Abstract*— This study demonstrated for the first time an in situ high-temperature fiber-optic Raman probe to study the structure of glass and slag samples at temperatures up to 1400 °C. A customized external telescope was integrated into a portable fiber-optic Raman probe to extend the optical working distance to allow the probe to work in a high-temperature environment. Three samples were evaluated to demonstrate the functionality of the high-temperature fiber-optic Raman probe. Room temperature and high-temperature Raman spectra were successfully collected and analyzed. In addition, a deconvolution algorithm was used to identify peaks in the spectrum that could then be related to the molecular structure of components in each sample. This flexible and reliable high-temperature Raman measurement method has great potential for various applications, such as materials development, composition, and structure monitoring during high-temperature processing, chemical identification, and process monitoring in industrial production.**

***Index Terms*— High-temperature Raman spectroscopy, in situ Raman, optical fiber sensor.**

I. Introduction

WHEN photons of light interact with a molecule, most photons are impacted by slight density fluctuations that change the direction of the photon, forming Rayleigh scattering. However, some small number of photons also change their frequency through Raman scattering [1]. The intensity of Raman scattered light is from 10^{-6} to 10^{-10} of the total scattered light intensity. Raman scattering arises from energy exchange between photons and molecules, which changes the energy of the photons [2]. These scattered photons enter different vibrational states specific to a molecule's chemical bonding and symmetry. Therefore, Raman scattering is known as a fingerprinting technique for diagnosing chemical substances, providing a tool for chemical structure investigation and molecular structure identification [3]. With the introduction of lasers, a powerful supply of high-quality, stable, high-intensity monochromatic laser light has become available, providing a great impetus to study Raman scattering and its applications for various conditions. As a result, the benchtop Raman system was developed. Consequently, Raman spectroscopy has been applied to various fields such as chemistry, physics, biology, and medicine [4], [5], [6]. Even in civil engineering, Raman spectroscopy has been applied to detect the chemical properties of concrete materials in hydration or carbonation reactions [7], [8]. In addition, Raman spectroscopy is valuable for qualitative and highly quantitative analysis and determining molecular structures [9], [10]. Although the benchtop Raman system has the advantage of high precision and accuracy, the disadvantages are obvious. First, the complicated equipment is unsuitable for performing on-line measurements in real-time. Second, the benchtop Raman system has specific requirements related to the sample size. As a result, special preparation is required for large samples, and non-destructive measurement cannot be achieved. However, on-line and real-time diagnoses for biochemical, medical, and material science applications are essential to scientific research. Therefore, a portable fiber-optic Raman sensor has been developed to allow the properties of materials to be studied in real-time.

Several fiber-optic Raman sensor designs have been reported for various applications. One study has shown that fiber-optic Raman sensors can be applied as indicators for composition detection in hydrocarbon mixtures [11]. Researchers tested and analyzed the Raman spectral intensity and area and claimed that the developed sensor is capable of monitoring methanol and ethanol in water and gasoline solutions. More fiber-optic Raman probes have been investigated and dedicated to real-time detection in vivo [12], [13], [14]. One such study reported a compact fiber-optic probe for in vivo measurement of near-infrared Raman spectra of human cervical tissue for clinical diagnosis of cervical precancerous lesions [15]. The comparison spectral results of the Raman spectrometer and the fiber-optic probe were also well interpreted. The low collection efficiency of the fiber-optic Raman sensors led to the development of a beveled fiber-optic confocal Raman probe [16]. A spherical lens was coupled to the fiber end to focus the light into a tiny spot. By selecting the appropriate fiber-optic spherical lens and beveled angle of the collection fibers, the design of the confocal Raman probe can be optimized to maximize superficial tissue Raman measurements

Manuscript received 10 September 2022; revised 15 January 2023; accepted 27 January 2023. Date of publication 13 February 2023; date of current version 24 February 2023. This work was supported by the U.S. Department of Energy's Office of Energy Efficiency and Renewable Energy (EERE) through the Advanced Manufacturing Office (AMO) under Award DE-EE0009392 and Award DE-EE0009119. The Associate Editor coordinating the review process was Dr. Alessio De Angelis. *(Corresponding author: Jie Huang.)*

Bohong Zhang, Rex E. Gerald II, and Jie Huang are with the Department of Electrical and Computer Engineering, Missouri University of Science and Technology, Rolla, MO 65409 USA (e-mail: jieh@mst.edu).

Hanok Tekle, Ronald J. O'Malley, and Jeffrey D. Smith are with the Department of Material Science and Engineering, Missouri University of Science and Technology, Rolla, MO 65409 USA.

Digital Object Identifier 10.1109/TIM.2023.3244238

of epithelial tissue. Fiber-optic Raman probes have been widely used in biochemistry and medicine. However, the properties of the fiber materials limit the extension of fiber-optic Raman probes in some materials science applications, such as in situ high-temperature studies. Novel materials have been developed by high-temperature heat treatments and understanding how the chemical composition changes in real-time during high-temperature reactions could be a transformative breakthrough for materials science research. As shown in Table I, early studies reported Raman spectra collected from quenched flux and slag samples [28], [29]. The previous studies were valuable to flux and slag materials research. However, Raman data were not recorded for molten state samples in real-time, which would have influenced the accuracy of the analyses. Other studies reported in situ Raman spectra of silica glasses in the range from room temperature to the glass transition temperature, and beyond to 1950 K for supercooled liquids [17], [18]. These studies used a new wire-loop heating technique to heat samples to elevated temperatures. However, the reported 0.5–0.8 mm in diameter micro heating one-turn coil that was employed as the heating system significantly limited researchers in their studies of small, droplet-size samples. Furthermore, Raman spectra were collected using a benchtop (non-portable) Raman system, which limits the applicability for applications at industrial work sites.

In this study, a fiber-optic Raman probe was combined with the concept of high-temperature Raman spectroscopy to perform in situ high-temperature Raman analysis. A customized external telescope was designed and embedded at the end of the Raman probe to extend the working distance of the probe from 0.8 to 3 cm, protecting the probe from the high-temperature environment for in situ studies. Three high melting temperature samples were prepared and heated to 1400 °C to perform high-temperature experiments. Raman spectra were successfully collected from room temperature to 1400 °C using the in situ fiber-optic Raman probe. The room and high-temperature Raman spectra are compared and discussed. Finally, the deconvolution algorithm applied to analyze and deconvolute the Raman spectra showed promising results. This in situ fiber-optic Raman probe will be a revolutionary step forward for real-time high-temperature studies in materials science and many other fields.

II. Fiber-Optic Raman Probe Configuration

The fiber-optic Raman probe (Inphotonics, RPP532/11-5C) was constructed with a main optical body and an extension tip holding the final focusing lens. The probe is coupled to the excitation source and a spectrometer via two separate optical fibers, allowing remote measurement of samples. Each fiber-optic subunit is housed in a protective polyurethane jacket. An excitation fiber with a core diameter of 105 μm and a collection fiber with a core diameter of 100 μm were employed inside the probe, as shown in Fig. 1. Inside the fiber-optic Raman probe, micro-optic components were utilized to deliver the laser excitation to the sample and collect scattered light, resulting in a compact probe head that

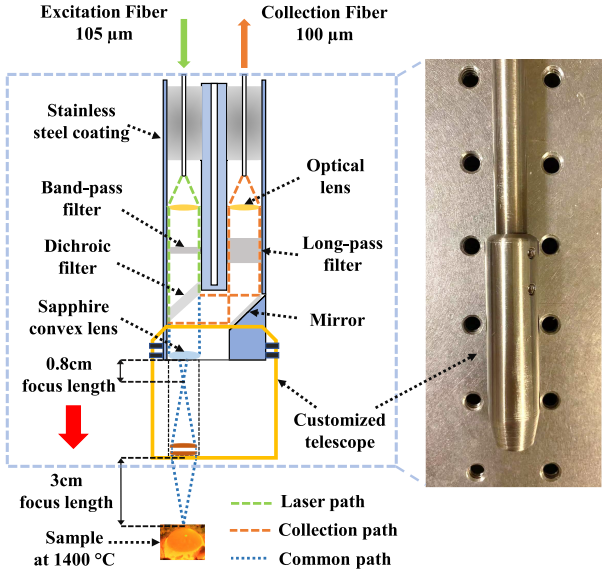

Fig. 1. Schematic of in situ fiber-optic Raman probe with the customized extremal telescope (left). Image of the in situ fiber-optic Raman probe with the customized external telescope (right). The customized external telescope provides a 3 cm working distance, which allows the probe to work in a high-temperature environment and long-time detection.

is optically coupled to the laser source and spectrograph. All the free-space optical components are mounted and aligned inside a rigid stainless-steel probe housing to avoid measurement errors from temperature-induced mechanical distortions. Through the efficient use of bandpass, dichroic, and edge filters for separating the excitation and scattered light, a 180° sampling geometry was obtained. The backscattering collection geometry allows for easy sample alignment and provides optimum throughput because of the overlap between the excitation and collection cones. Another advantage of using a second fiber for signal collection is to remove the inelastic background signal from the excitation fiber itself. Based on the Raman probe's lens design, the default working distance is 8 mm. Moreover, the laser spot size could be varied based on the transmission properties of the sample under measurement. The smallest spot size employed was around 100 μm when the distance of the sample to the probe was about 8 mm. Each fiber-optic subunit is provided in a protective polyurethane jacket. The outer jacketing material of the Raman probe is 316 stainless steel which provides a 650 °C maximum temperature threshold for high-temperature usage.

Common glass materials, slags, and fluxes are processed at temperatures as high as 1300 °C–1400 °C. Because of this, the idea of using an external telescope to enlarge the probe's working distance to isolate the probe from the heating environment was proposed. An external telescope protected by a stainless-steel jacket (functional to 900 °C) was custom designed to expand the capability of the Raman probe to higher temperatures. As shown in Fig. 1, the excitation light can only be focused to 0.8 cm after passing through the sapphire lens in the original Raman probe design. After applying the telescope attachment (yellow block), the two additional optical lenses first collimate the light and then focus it, increasing the

TABLE I
COMPARISON OF THE ADVANTAGES AND DISADVANTAGES OF THE PREVIOUS METHODS WITH THE PROPOSED METHOD

	Previous methods [17], [18], [28], [29]	Proposed method
Advantages	• Achieve precisely localized testing position by employing a bench top Raman system (~1 μm position resolution)	• Non-destructive *in situ* analysis • Direct measurements: no sample preparation required • Real-time measurements under high-temperature conditions • Potential use at on-site systems in industry
Disadvantages	• Complex sample preparation • Sample size limitation • Non-portable system	• Localized sample testing area is large due to the larger laser spot size (~100 μm)

optical path's focusing distance to 3 cm without energy loss. The increased working distance of the Raman probe provided the opportunity for performing subsequent high-temperature experiments.

III. HIGH-TEMPERATURE FIBER-OPTIC RAMAN SYSTEM

In the high-temperature fiber-optic Raman system shown in Fig. 2, a laser and a spectrometer were connected at each end of the Raman probe. A 532 nm laser (green laser) was used as the excitation source to provide the best Raman performance for the tested sample. In addition, a QE-Pro spectrometer was employed to collect Raman spectra with a spectral resolution of 3 cm^{-1}. An induction coil furnace was used to provide high-temperature continuous heating during the experiment.

The fiber-optic Raman probe was mounted on a stand with a proper probe working distance, as shown in Fig. 2. A K-type thermocouple was fixed adjacent to the Raman probe to monitor its ambient temperature in real-time. After repeated experiments, the temperature in the probe area was about 150 °C at a controlled distance of 3 cm from the sample. In addition, real-time temperature data was sampled and recorded using a data logger. Two types of graphite crucibles were used for the high-temperature experiments. The base crucible was surrounded by an aluminosilicate refractory and fixed in the induction coil. The working crucible was embedded into the base crucible as a container for heating samples. An S-type thermocouple installed in direct contact with the working crucible was used to control the temperature of the sample. After repeated experimental measurements, the heating system was found to be consistently capable of heating samples to 1400 °C for 10–15 min. Therefore, the real-time high-temperature Raman spectra were able to be collected repeatedly at the same temperature condition to improve the accuracy of the experiment.

IV. MATERIALS PREPARATION

As shown in Table II, to better demonstrate the capabilities of the high-temperature fiber-optic Raman probe for materials science research, three samples with high melting temperatures were prepared for testing, a electric arc furnace (EAF) slag, a mold flux, and a bio glass (45S5) sample. The melting temperature of the EAF slag and mold flux samples ranged from 1350 °C to 1400 °C. The melting point of bio glass was between 1250 °C to 1300 °C. To thoroughly investigate the Raman spectra of the samples in the liquid state, the heating temperature was set to 1400 °C for the EAF slag and mold flux and 1300 °C for the bio glass to ensure the materials were fully melted. The melting was also confirmed visually.

V. RESULTS AND DISCUSSION

It is well known that thermal radiation can affect Raman scattering at high temperatures [18], [19], [20]. The energy level of thermal radiation is closely related to temperature. Therefore, a strong thermal radiation signal may significantly affect the Raman signal of the test sample. However, the energy level of the thermal radiation can be considered the same at the same temperature condition. Therefore, if all Raman spectra are examined at the same temperature, the problems associated with the intrinsic temperature dependence of Raman scattering can be eliminated. This research proposed a background subtraction method to eliminate the background thermal radiation signal. In the high-temperature experiments, an empty furnace was first heated to 1400 °C and held to ensure thermal stability. Then, the fiber-optic Raman probe was moved to the measurement area for background signal acquisition. Subsequently, the prepared sample was poured into the crucible for sintering and melting. Finally, a second Raman signal was acquired when the sample was completely melted. To improve the signal-to-noise ratio of the actual sample Raman signal, the acquisition integration time was set to 2–5 s. Ten sets of Raman spectra were acquired for each temperature and then averaged to further reduce the interference of the noise signals, addressing the uncertainties for the signal collection.

The first sample tested by the in situ fiber-optic Raman probe was an EAF slag generated during the EAF steel-making process. According to previous studies, the viscosity of this molten slag is strongly correlated with the Raman signal in the Q region at 800–1050 cm^{-1} [21], [22]. Therefore, the Raman spectra of the Q region in the EAF slag were investigated in this research. The Raman spectra were successfully collected at room temperature and 1400 °C, as shown in Fig. 3. The raw Raman spectra showed that the sample had a strong carbonate peak (1083 cm^{-1}) before being heated. However, after the slag was heated to the liquid state (1400 °C), the carbonate Raman peak intensity decreased dramatically due to the carbonate decomposition in the high-temperature environment [23]. The Raman signal in

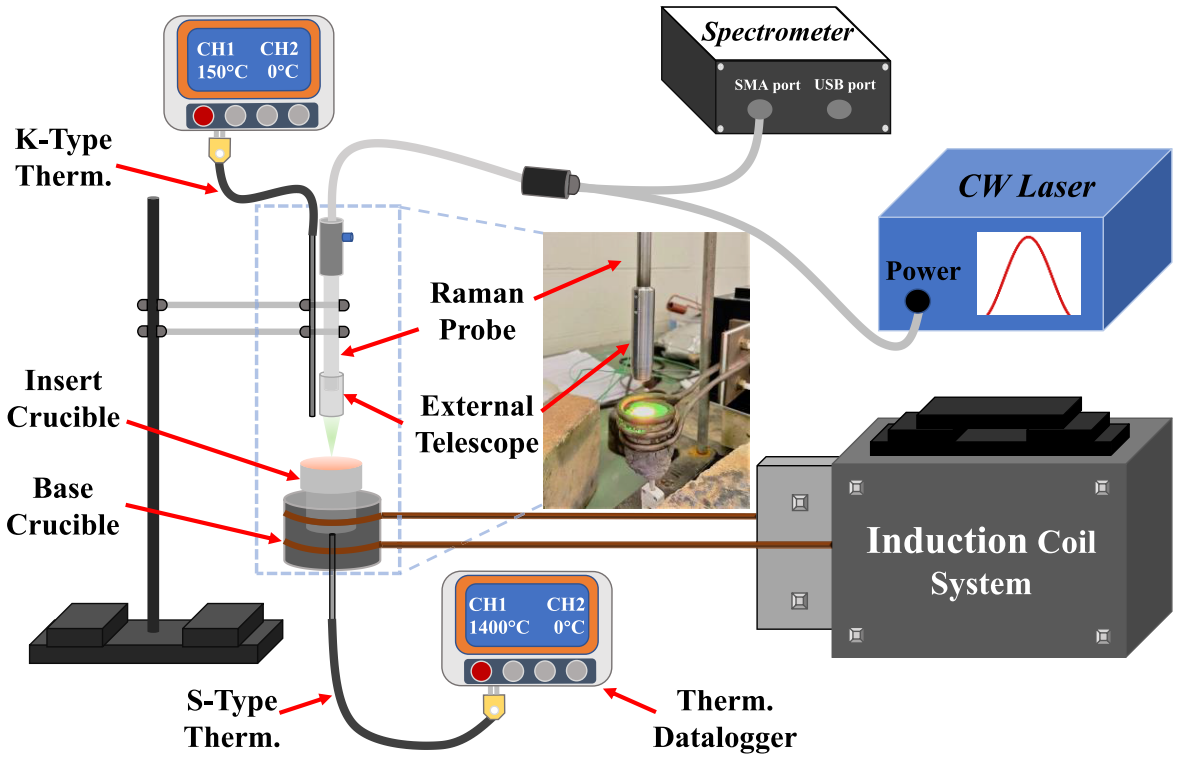

Fig. 2. Schematic of in situ high-temperature fiber-optic Raman system with an induction coil system for high-temperature experiments. Image of the in situ fiber-optic Raman probe in high-temperature experiment (middle).

TABLE II
CHEMICAL COMPOSITION OF THREE TESTING SAMPLES (EAF SLAG, MOLD FLUX, AND BIO GLASS) USED IN THIS STUDY

EAF slag (wt%)	SiO_2 17	CaO 34	Al_2O_3 14.5	Fe_2O_3 26	MgO 5	Mn_2O_3 3.5
Mold flux (wt%)	SiO_2 42.87	CaO 35.87	Al_2O_3 4.69	Na_2O 7.5	Fluoride 9.07	
Bio glass (wt%)	SiO_2 45	CaO 24.5	Na_2O 24.5	P_2O_5 6		

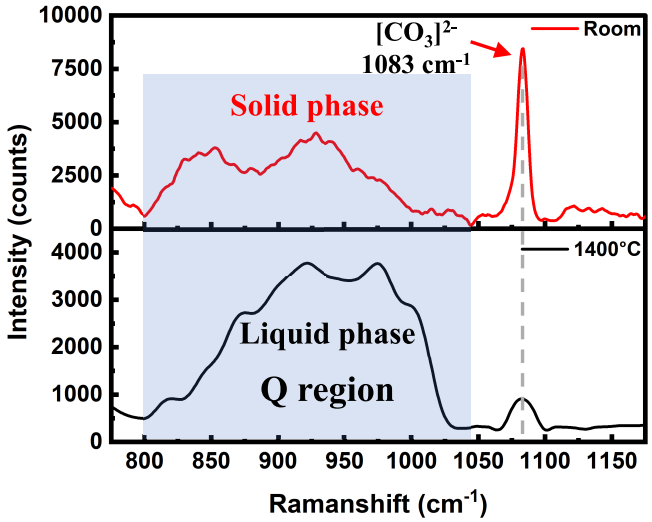

Fig. 3. Raman spectra of the EAF slag sample, collected under room (red) and 1400 °C (black) temperature conditions. The intensity of the Raman peak at 1083 cm^{-1} substantially decreased at higher temperatures indicating decomposition of carbonates in the sample.

the Q region at room temperature changed dramatically at high temperatures. Multiple compounds or molecular bonds have a close wavenumber, often resulting in overlapping peaks in complex samples. Therefore, deconvolution methods are widely used in Raman spectroscopy for further chemical analysis of a broad range of Raman spectra [24], [25]. In the deconvolution algorithm applied in this article, a Gaussian function was used for curve fitting. Fig. 4 shows the deconvolution results of Raman spectra at room and high temperatures for the EAF slag. Based on the Raman spectral data summarized in previous experiments, the Q region signals were deconvoluted into Q^0 $(Si_2O_4)^{4-}$, Q^1 $(Si_2O_7)^{6-}$, Q^2 $(SiO_3)^{2-}$, and Q^3 $(Si_2O_5)^{2-}$ [21].

By comparing the results after deconvolution of the EAF slag samples at both temperatures, it is observed that the Raman signal in the Q region is shifted to the right after heating. The following findings were obtained after comparing the Raman deconvolution data at room and high temperatures. First, there was no Q^3 peak found in the room temperature deconvolution Raman results. The reason is that the high content of Fe_2O_3 (26 wt%) and high basicity ($CaO/SiO_2 = 2$) in the slag provide a sufficient amount of free oxygen ions to break up Q^3 into Q^2, Q^1, and Q^0 [22]. However, when the sample was heated to a molten state of 1400 °C, a small Q^3 peak was observed. Second, the increase in Q^2 bonding

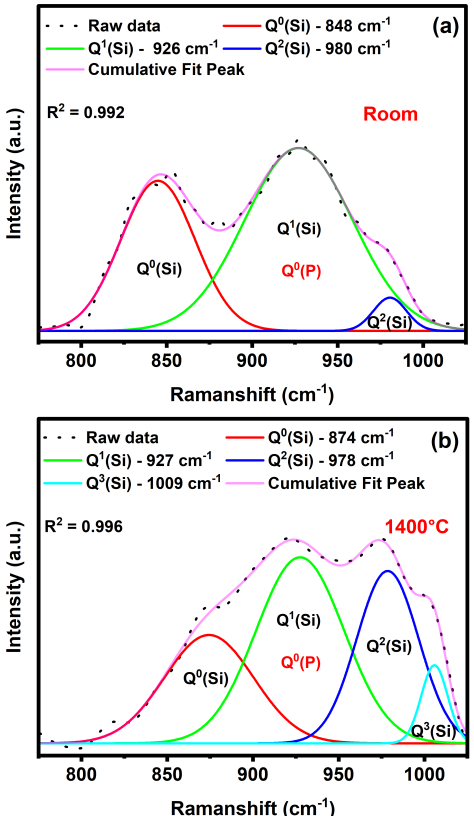

Fig. 4. Deconvolution result of the EAF slag Raman spectra. (a) Deconvolution result at room temperature. (b) Deconvolution result at 1400 °C. Compared with the Raman spectra of room temperature, the overall Q region signal appeared right shifted for the Raman spectra of 1400 °C.

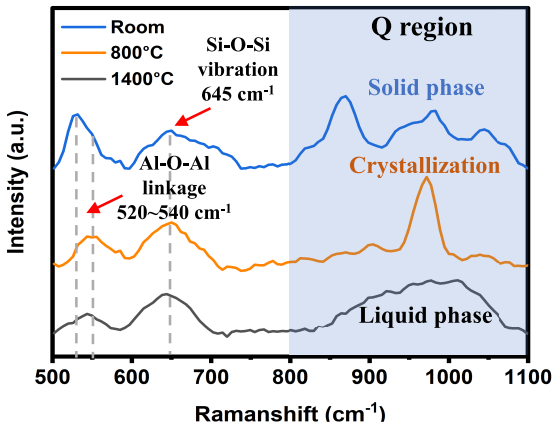

Fig. 5. Raman spectra of the mold flux at room (blue), 800 °C (yellow), and 1400 °C (black) temperature conditions. The Raman signal of Al–O–Al and Si–O–Si were found in all three temperature conditions. Q region Raman signal appeared to have a significant change in different temperature conditions.

observed after heat treatment was at the expense of the decrease in all other Q^n bonds, suggesting that the crystalline phase is a ring silicate. This conclusion is confirmed by previous studies on quenched and cooled samples [26], [27].

The second sample tested by the in situ fiber-optic Raman probe was a mold flux, a Ca–Si–Al–oxyfluoride glass used to control the heat transfer and lubricate the mold in the continuous casting process. The Raman spectra

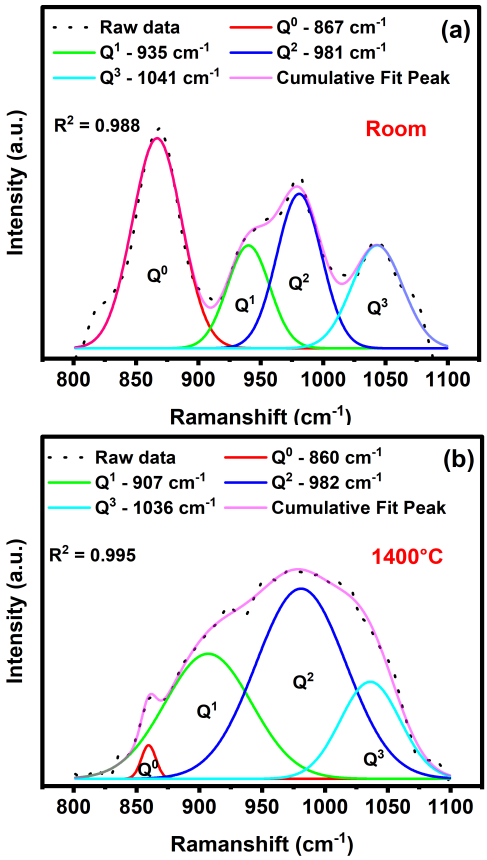

Fig. 6. Deconvolution result of the mold flux Raman spectra. (a) Deconvolution result at room temperature. (b) Deconvolution result at 1400 °C. Compared with the deconvolution result for room temperature, the Q^3/Q^2 ratio decreases and the Q^3/Q^0 increases with increasing temperature.

were collected for three different temperature conditions, as shown in Fig. 5. Besides the Q region Raman signal, two more significant Raman peaks were found in 520–540 and 645 cm^{-1}, representing Al–O–Al and Si–O vibration bonds [28], [29]. According to the high melting point of alumina and silicon, the peaks at 520–540 and 645 cm^{-1} were very robust, and no significant change with the temperature increase was observed. However, the variation of the Q region Raman spectra from 800 to 1100 cm^{-1} with temperature is evident, representing three states of the mold flux: solid state, crystallized state, and liquid or molten state.

Again, the deconvolution analysis was performed for the room and high-temperature mold flux Raman data, as shown in Fig. 6. The four separate Raman peaks Q^0, Q^1, Q^2, and Q^3 were successfully resolved for both Raman spectra. The most prominent Q^0 peak in the Raman spectra indicates a large number of silicate monomers in the sample at room temperature. With heating, a large number of monomers recombine with oxygen to form chains and sheets, i.e., Q^2 and Q^3. Then, the Q^0 Raman peak significantly decreased, and the Q^2 Raman peak was found to dominate in the 1400 °C Raman spectra, indicating that the molten flux sample contains silicate chains. In addition, an increase in the degree of polymerization is associated with higher melting temperatures and higher mechanical strength. In a previous study, the Q^3/Q^2 ratio was found as a good indicator of

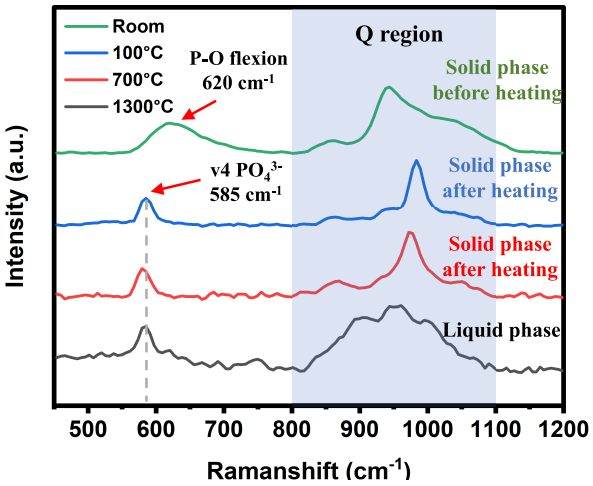

Fig. 7. Raman spectra of the bio glass at room (green), 100 °C (blue), 700 °C (red), and 1300 °C (black) temperature conditions. A new Raman peak was found at 585 cm^{-1} after temperatures above 100 °C. Q region Raman signal changed significantly in different temperature conditions.

the degree of polymerization [30]. After analyzing the data from this preliminary study, the Q^3/Q^2 ratio decreases with increasing temperature, which showed an agreement with previous research [30]. Additionally, it is noted that the Q^3/Q^0 ratio increases with increasing temperature because silicate monomers recombine with oxygen to form sheets. Therefore, more experiments are needed to optimize the correlation in future studies.

The last sample investigated with the in situ fiber-optic Raman probe was a bioactive glass (45S5), which is applied as an implant device in the human body to repair and replace diseased or damaged bones. Four Raman spectra were successfully observed at room temperature, 100 °C, 700 °C, and 1300 °C, as shown in Fig. 7. Room temperature Raman spectra were first acquired before the sample was heated. Afterward, the sample was heated to 1300 °C, melted, and the Raman spectra were acquired. Then, the furnace temperature was adjusted to 700 °C and kept at a constant temperature. Once the temperature was stabilized, the Raman spectra at 700 °C were acquired. Finally, the temperature was lowered to 100 °C, and the Raman spectra were acquired. This heating protocol was employed to mitigate the influence of metastable crystalline phases on the analysis. The room temperature Raman spectra show two principal bands: 620 cm^{-1} as the P–O flexion band and within the 800–1100 cm^{-1} range as the Q region [31]. However, the high-temperature Raman spectra at 100 °C, 700 °C, and 1300 °C showed that the P–O flexion band disappeared at 620 cm^{-1} after heating. Instead, a new Raman peak was found at 585 cm^{-1}, which likely represents the v4 PO_4^{3-} that contains contributions from acid phosphate (HPO_4) and octacalcium phosphate (OCP) [32], [33]. In addition, the Raman signal of the Q region changes dramatically at different temperatures. There is an overall shift of the spectral features in the Q region to a higher wavenumber when the sample is heated from room temperature to 700 °C. When the temperature exceeds the sample's melting point at 1300 °C, the Q region changes significantly in the range of 950–1050 cm^{-1}.

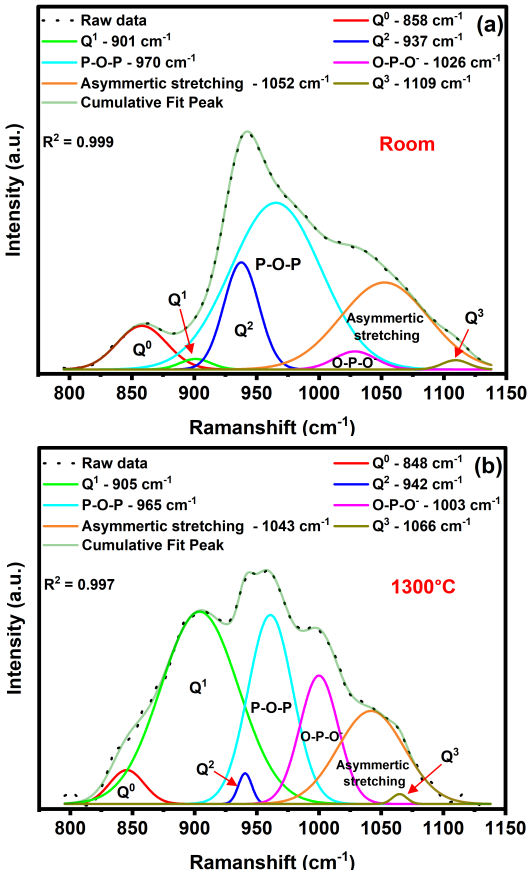

Fig. 8. Deconvolution result of the bio glass Raman spectra. (a) Deconvolution result at room temperature. (b) Deconvolution result at 1300 °C. Seven Raman peaks were deconvoluted from room and 1300 °C Raman signal.

To further understand the relationship between chemical bonds and the Raman spectra of bio glass, the Raman spectra at room and high temperatures were deconvoluted, applying peaks identified from an earlier study on the bio glass [34]. Seven major Raman peaks were deconvoluted, and the attributions considered for the peak fitting were as follows: Q^0 at 864 cm^{-1}; Q^1 at 906 cm^{-1}; Q^2 at 944 cm^{-1}; P–O–P stretching at 974 cm^{-1}; O–P–O-stretching of the P_2O_5 sheet unit at 1008 cm^{-1}; asymmetric stretching of the bridge oxygen in all Q species; and the symmetric stretching of Q^3 at 1086 cm^{-1}, as shown in Fig. 8. Bioactive glasses are usually formed from open silicate networks, i.e., interconnected silicate chains and rings that result in porous materials, while other silicate networks (sheets) are less porous (denser) and occur infrequently. The room-temperature Raman results obtained by deconvolution were then compared with previous research results and found to be in good agreement [34]. In the future, more experiments will be needed to investigate the changes in molecular bonds in bio glass samples at high temperatures. Nevertheless, this method of in situ high-temperature fiber-optic Raman probe opens a new chapter for future materials science research.

VI. Conclusion

In summary, a fiber-optic Raman probe has been demonstrated to perform real-time in situ high-temperature Raman spectroscopy. Combining a fiber-optic probe and the

high-temperature Raman spectroscopy is unique, and this is the first demonstration of use in practical remote sensing applications. Furthermore, an external telescope was designed to increase the working distance of the fiber-optic Raman probe to allow real-time Raman analysis to be performed on large samples at high temperatures. The extended working distance successfully demonstrated the capabilities of the fiber-optic Raman probe for a high-temperature environment measurement and long-time detection. Three high melting point glass and slag samples were prepared for high-temperature Raman testing. The Raman spectra at room temperature and high temperature were successfully acquired. A deconvolution algorithm was successfully employed to identify the unique chemical bonds contributing to the total Raman spectral response. The experimental results were compared with results from previous studies of quenched glass samples and were found to be in good agreement. The experimental results and techniques presented in this work can serve as a roadmap for investigating material properties under high-temperature conditions, which may facilitate the use of high-temperature fiber-optic Raman spectroscopy in metal fabrication, steelmaking, and other high-temperature related materials research.

ACKNOWLEDGMENT

The views and opinions of authors expressed herein do not necessarily state or reflect those of the United States Government or any agency thereof.

REFERENCES

[1] L. A. Lyon et al., "Raman spectroscopy," *Anal. Chem.*, vol. 70, no. 12, pp. 341–362, 1998.

[2] S. P. Mulvaney and C. D. Keating, "Raman spectroscopy," *Anal. Chem.*, vol. 72, no. 12, pp. 145–158, 2000.

[3] Y. C. Cao, R. Jin, and C. A. Mirkin, "Nanoparticles with Raman spectroscopic fingerprints for DNA and RNA detection," *Science*, vol. 297, pp. 1536–1540, Aug. 2002.

[4] G. C. Green, A. D. C. Chan, B. S. Luo, H. Dan, and M. Lin, "Identification of listeria species using a low-cost surface-enhanced Raman scattering system with wavelet-based signal processing," *IEEE Trans. Instrum. Meas.*, vol. 58, no. 10, pp. 3713–3722, Oct. 2009.

[5] H. J. Butler et al., "Using Raman spectroscopy to characterize biological materials," *Nature Protocols*, vol. 11, no. 4, pp. 664–687, 2016.

[6] R. Song, W. Chen, D. Yang, H. Shi, R. Zhang, and Z. Wang, "Aging assessment of oil–paper insulation based on visional recognition of the dimensional expanded Raman spectra," *IEEE Trans. Instrum. Meas.*, vol. 70, pp. 1–10, 2021.

[7] S. Martinez-Ramirez, M. Frías, and C. Domingo, "Micro-Raman spectroscopy in white Portland cement hydration: Long-term study at room temperature," *J. Raman Spectrosc.*, vol. 37, no. 5, pp. 555–561, 2006.

[8] J. Bensted, "Uses of Raman spectroscopy in cement chemistry," *J. Amer. Ceram. Soc.*, vol. 59, nos. 3–4, pp. 140–143, Mar. 1976.

[9] Z. Liu et al., "Revealing the molecular structure of single-molecule junctions in different conductance states by fishing-mode tip-enhanced Raman spectroscopy," *Nature Commun.*, vol. 2, no. 1, p. 305, May 2011.

[10] D. B. Schuepfer et al., "Assessing the structural properties of graphitic and non-graphitic carbons by Raman spectroscopy," *Carbon*, vol. 161, pp. 359–372, May 2020.

[11] S. K. Khijwania, V. S. Tiwari, F.-Y. Yueh, and J. P. Singh, "A fiber optic Raman sensor for hydrocarbon detection," *Sens. Actuators B, Chem.*, vol. 125, no. 2, pp. 563–568, Aug. 2007.

[12] P. Žuvela, K. Lin, C. Shu, W. Zheng, C. M. Lim, and Z. Huang, "Fiber-optic Raman spectroscopy with nature-inspired genetic algorithms enhances real-time in vivo detection and diagnosis of nasopharyngeal carcinoma," *Anal. Chem.*, vol. 91, no. 13, pp. 8101–8108, Jul. 2019.

[13] M. Plesia et al., "In vivo fiber optic Raman spectroscopy of muscle in preclinical models of amyotrophic lateral sclerosis and Duchenne muscular dystrophy," *ACS Chem. Neurosci.*, vol. 12, no. 10, pp. 1768–1776, May 2021.

[14] H. P. S. Heng, C. Shu, W. Zheng, K. Lin, and Z. Huang, "Advances in real-time fiber-optic Raman spectroscopy for early cancer diagnosis: Pushing the frontier into clinical endoscopic applications," *Transl. Biophotonics*, vol. 3, no. 1, Mar. 2021, Art. no. e202000018.

[15] A. Mahadevan-Jansen, M. F. Mitchell, N. Ramanujam, U. Utzinger, and R. Richards-Kortum, "Development of a fiber optic probe to measure NIR Raman spectra of cervical tissue in vivo," *Photochem. Photobiol.*, vol. 68, no. 3, pp. 427–431, Sep. 1998.

[16] J. Wang, M. S. Bergholt, W. Zheng, and Z. Huang, "Development of a beveled fiber-optic confocal Raman probe for enhancing in vivo epithelial tissue Raman measurements at endoscopy," *Opt. Lett.*, vol. 38, no. 13, p. 2321, Jun. 2013.

[17] P. F. Mcmillan, B. T. Poe, P. H. Gillet, and B. Reynard, "A study of SiO_2 glass and supercooled liquid to 1950 K via high-temperature Raman spectroscopy," *Geochimica et Cosmochimica Acta*, vol. 58, no. 17, pp. 3653–3664, Sep. 1994.

[18] I. Daniel, P. Gillet, B. Poe, and P. Mcmillan, "In-situ high-temperature Raman spectroscopic studies of aluminosilicate liquids," *Phys. Chem. Minerals*, vol. 22, no. 2, pp. 74–86, Mar. 1995.

[19] B. T. Bowie, D. B. Chase, P. R. Griffiths, and DuPont, "Factors affecting the performance of bench—Top Raman spectrometers—Part II: Effect of sample," *Appl. Spectrosc.*, vol. 54, no. 6, pp. 200A–207A, Jun. 2000.

[20] B. O. Mysen and J. D. Frantz, "Raman spectroscopy of silicate melts at magmatic temperatures: Na_2O-SiO_2, K_2O-SiO_2 and Li_2O-SiO_2 binary compositions in the temperature range 25–1475°C," *Chem. Geol.*, vol. 96, nos. 3–4, pp. 321–332, Apr. 1992.

[21] X. Shen, M. Chen, N. Wang, and D. Wang, "Viscosity property and melt structure of CaO-MgO-SiO_2-Al_2O_3-FeO slag system," *ISIJ Int.*, vol. 59, no. 1, pp. 9–15, 2019.

[22] K. X. Jiao, J. L. Zhang, Z. Y. Wang, C. L. Chen, and Y. X. Liu, "Effect of TiO_2 and FeO on the viscosity and structure of blast furnace primary slags," *steel Res. Int.*, vol. 88, no. 5, May 2017, Art. no. 1600296.

[23] W. Li et al., "Raman characterization of aligned carbon nanotubes produced by thermal decomposition of hydrocarbon vapor," *Appl. Phys. Lett.*, vol. 70, no. 20, pp. 2684–2686, May 1997.

[24] R. K. Brow, "Review: The structure of simple phosphate glasses," *J. Non-Crystalline Solids*, vols. 263–264, pp. 1–28, Mar. 2000.

[25] B. O. Mysen, J. R. Frederick, and V. David, "The structural role of phosphorus in silicate melts," *Amer. Mineralogist.*, vol. 66, nos. 1–2, pp. 106–117, 1981.

[26] R. A. da Silveira, L. D. L. Evaristo, F. L. Faita, and S. Buchner, "Effect of high pressure and high temperature on the $Na_2O \cdot 2CaO \cdot 3SiO_2$ glass-ceramic's structural properties," *J. Non-Crystalline Solids*, vol. 570, Oct. 2021, Art. no. 121026.

[27] R. X. Fischer and E. Tillmanns, "Revised data for combeite, $Na_2Ca_2Si_3O_9$," *Acta Crystallographica Sect. C Crystal Struct. Commun.*, vol. 43, no. 9, p. 1852, Sep. 1987.

[28] W. Yan, G. Zhang, and J. Li, "Viscosity and structure evolution of CaO–SiO_2-based mold fluxes with involvement of CaO–Al_2O_3-based tundish fluxes," *Ceram. Int.*, vol. 46, no. 9, pp. 14078–14089, Jun. 2020.

[29] J. Gao, G. Wen, T. Huang, P. Tang, and Q. Liu, "Effects of the composition on the structure and viscosity of the CaO–SiO_2-based mold flux," *J. Non-Crystalline Solids*, vol. 435, pp. 33–39, Mar. 2016.

[30] J. H. Park, "Composition–structure–property relationships of CaO–MO–SiO_2 (M=Mg^{2+}, Mn^{2+}) systems derived from micro-Raman spectroscopy," *J. Non-Crystalline Solids*, vol. 358, no. 23, pp. 3096–3102, Dec. 2012.

[31] M. S. Araujo, J. F. Bartolomé, and S. Mello-Castanho, "Tribological and mechanical behaviour of 45S5 bioglass-based compositions containing alumina and strontium," *Ceram. Int.*, vol. 46, no. 15, pp. 24347–24354, Oct. 2020.

[32] E. A. Taylor and E. Donnelly, "Raman and Fourier transform infrared imaging for characterization of bone material properties," *Bone*, vol. 139, Oct. 2020, Art. no. 115490.

[33] G. Penel, C. Delfosse, M. Descamps, and G. Leroy, "Composition of bone and apatitic biomaterials as revealed by intravital Raman microspectroscopy," *Bone*, vol. 36, no. 5, pp. 893–901, May 2005.

[34] M. S. Araujo, A. C. Silva, J. F. Bartolomé, and S. Mello-Castanho, "Structural and thermal behavior of 45S5 bioglass-based compositions containing alumina and strontium," *J. Amer. Ceram. Soc.*, vol. 103, no. 6, pp. 3620–3630, 2020.

Bohong Zhang received the Ph.D. degree in electrical engineering from the Missouri University of Science and Technology, Rolla, MO, USA, in 2022.

He is currently a Post-Doctoral Research Fellow with the Missouri University of Science and Technology. His current research interests include developing optical sensors and instrumentation for energy, biomedical sensing, and harsh environments.

Hanok Tekle received the B.S. degree in metallurgical engineering from the Missouri University of Science and Technology, Rolla, MO, USA, in 2020, where he is currently pursuing the Ph.D. degree in material science.

His current research interests include applied distributed fiber optic sensors in steelmaking and high-temperature Raman spectroscopy work with slag systems.

Ronald J. O'Malley is currently the F. Kenneth Iverson Chair Professor of steelmaking technologies with the Department of Metallurgical Engineering, Missouri University of Science and Technology, Rolla, MO, USA. He is also the Director of the Kent D. Peaslee Steel Manufacturing Research Center (PSMRC), Rolla, which is an industry-supported consortium with 19 industry members that support ∼U.S. $1M in research annually. He is also the PI of >U.S. $18M in research with the Department of Energy (DOE) and the Defense Logistics Agency (DLA) in areas of sensor development, hydrogen steelmaking, and electric furnace optimization. He has more than 30 years of experience in the metals manufacturing industry at Alcoa, Alcoa Center, New Kensington, PA, USA; Armco/AK Steel, Middletown, OH, USA; and Nucor Steel, LLC, Decatur, AL, USA. He has authored more than 150 journal and conference proceedings papers, over 70 invited and contributed presentations, and holds three U.S. patents. He is a Lecturer of several short courses in steel manufacturing, including the Brimacombe short course on Continuous Casting. His current research interests include H2 ironmaking, electric arc furnace (EAF) steelmaking, steel refining, clean steel processing and inclusion engineering, steel-refractory interactions, continuous casting, deformation processing, sensor development for harsh steelmaking environments, and new steel grade development.

Dr. O'Malley was the President of the Association for Iron and Steel Technology (AIST) from 2019 to 2021. He is an AIST Distinguished Member and a fellow.

Jeffrey D. Smith is currently a Professor of ceramic engineering with the Department of Materials Science and Engineering, Missouri University of Science and Technology, Rolla, MO, USA. His current research interests include high-temperature inorganic chemistry, materials characterization, high-temperature materials, and interactions between ceramics and molten materials.

Rex E. Gerald II received the B.A. degree (Hons.) in chemistry from The University of Chicago (UC), Chicago, IL, USA, in 1984, and a conjoint Ph.D. degree in physical chemistry from the University of Illinois Chicago (UIC), Chicago, and the Max Planck Institute (MPI), Heidelberg, Germany, in 1994.

He is currently a Research Professor with the Lightwave Technology Laboratory, Department of Electrical and Computer Engineering, Missouri University of Science and Technology (MS&T), Rolla, Mo, USA. He holds 26 U.S. patents and coauthored more than 80 publications from research investigations conducted at UC; UIC; MPI; Argonne National Laboratory, Lemont, IL, USA; and MS&T.

Jie Huang (Senior Member, IEEE) received the Ph.D. degree in electrical engineering from Clemson University, Clemson, SC, USA, in 2015.

He is currently the Roy A. Wilkens Endowed Associate Professor of electrical and computer engineering with the Missouri University of Science and Technology, Rolla, MO, USA. He has established the Lightwave Technology Laboratory (LTL), Rolla, MO, USA, with a strong track record of sustained research funding, high-quality journal publications, and state-of-the-art research infrastructures with cutting-edge capabilities. He has authored or coauthored over 100 refereed articles, 70 conference papers, one book chapter, and ten U.S. patent applications, all in the area of advanced sensors. His current research interests include the development of optical and microwave sensors and instrumentation for applications in energy, intelligent infrastructures, clean environments, biomedical sensing, and harsh environments.